CHEMISTRY
A EUROPEAN JOURNAL

DOI: 10.1002/chem.200903423

Study of the Light-Induced Spin Crossover Process of the $[Fe^{II}(bpy)_3]^{2+}$ Complex

Coen de Graaf*[a, b] and Carmen Sousa[c]

Abstract: Ab initio calculations have been performed on $[Fe^{II}(bpy)_3]^{2+}$ (bpy = bipyridine) to establish the variation of the energy of the electronic states relevant to light-induced excited-state spin trapping as a function of the Fe–ligand distance. Light-induced spin crossover takes place after excitation into the singlet metal-to-ligand charge-transfer (MLCT) band. We found that the corresponding electronic states have their energy minimum in the same region as the low-spin (LS) state and that the energy dependence of the triplet MLCT states are nearly identical to the ^{1}MLCT states. The high-spin (HS) state is found to cross the MLCT band near the equilibrium geometry of the MLCT states. These findings give additional support to the hypothesis of a fast singlet–triplet interconversion in the MLCT manifold, followed by a ^{3}MLCT–HS ($^5T_2$) conversion accompanied by an elongation of the Fe–N distance.

Keywords: ab initio calculations · magnetic properties · photochemistry · spin crossover · transition metals

Introduction

The phenomenon of spin crossover (SCO) in iron(II)-based molecular complexes has been extensively studied in recent years.[1] The conversion from a low-spin (LS) ground state to a high-spin (HS) excited state can be induced by a variation in temperature or by light irradiation, whereas the reverse process can, in addition, be triggered by changing the external pressure. Complexes showing a small zero-point energy difference between the HS and LS states (ΔE^0_{HL}), typically of the order of 0–1000 cm^{-1},[2,3] can exhibit thermal SCO, that is, an entropy-driven transition from the populated LS state at low temperatures to the HS state, populated at higher temperatures. The spin conversion from LS to HS states can also be optically triggered by photoirradiation based on the light-induced excited spin state trapping (LIESST) phenomenon.[4–7] At low temperatures, the HS state can be populated by irradiation of the system into the LS metal d–d or metal-to-ligand charge-transfer (MLCT) absorption bands, followed by a double intersystem crossing involving intermediate spin states.[6] The LS to HS spin transition is accompanied by a substantial elongation of the metal–ligand bond lengths. A large number of SCO complexes known to date contain Fe^{II} in a $3d^6$ electronic configuration and an N_6 nearly octahedral first coordination sphere. For these compounds the LS is a $^1A_1$ (t_2^6) state, the HS is a $^5T_2$ ($t_2^4e^2$) electronic state, and the variation in the Fe–N distances from the LS to the HS state is approximately 0.2 Å.[8] This elongation is explained by the promotion of two electrons from the nonbonding t_2 orbitals to the antibonding e orbitals under the spin transition. LS to HS SCO has been observed both in the solid state and in solution, although the most interesting properties for technical applications are related to cooperative phenomena in the solid state. However, the study of dilute systems is important to understand the fundamental intramolecular processes related to the spin transition.

The $[Fe^{II}(bpy)_3]^{2+}$ complex is found to be a LS system with $\Delta E^0_{HL} \approx 6000\ cm^{-1}$ and hence, thermal SCO cannot be induced for this compound. Nevertheless, LS to HS conversion can be optically triggered by the LIESST process. For

[a] Dr. C. de Graaf
Departament de Química Física i Inorgànica
Universitat Rovira i Virgili, c/Marcel·lí Domingo s/n
Campus Sescelades, 43007 Tarragona (Spain)
Fax: (+34) 977-55-9563
E-mail: coen.degraaf@urv.cat

[b] Dr. C. de Graaf
Institució Catalana de Recerca i Estudis Avançcats (ICREA)
Passeig Lluís Companys 23, 08010 Barcelona (Spain)

[c] Dr. C. Sousa
Departament de Química Física and
Insitut de Química Teòrica i Computacional Universitat de Barcelona
c/Martí i Franquès 1, 08028 Barcelona (Spain)

Supporting information for this article is available on the WWW under http://dx.doi.org/10.1002/chem.200903423.

$[Fe^{II}(bpy)_3]^{2+}$ in solution, the HS state relaxes nonradiatively to the LS ground state in less than 700 ps,[9,10] which is different to the light-induced HS states of other SCO materials for which the lifetime at low temperatures can be hours. For this reason, structural information is only available for the LS state, both in solid state[11] and in solution.[12] In both cases, the Fe–N distances are similar at approximately 1.97–1.98 Å. Only recently, Gawelda et al.[12,13] were able to confirm an elongation of the Fe–N distance of 0.2 Å for the HS state by picosecond X-ray absorption spectroscopy. This variation is similar to that found for other iron(II) SCO complexes, indicating that the driving force for the HS–LS relaxation is determined by the energetics rather than by structural changes.

The optical absorption spectrum of $[Fe^{II}(bpy)_3]^{2+}$ shows an intense and broad band centered at 523 nm assigned to the singlet MLCT (^{1}MLCT) states. The relaxation process from this state to the HS state occurs with almost 100% quantum efficiency and ultrafast laser spectroscopy shows that this process is complete in less than 1 ps.[14] Furthermore, ^{3}MLCT states were clearly observed in the measurements, suggesting a crucial role of these states in the deactivation. Other authors proposed that the intermediate states could be a mixture of all excited ligand-field states lying between the ^{1}MLCT state and the $^5T_2$ state.[9] Recent studies of the dynamics of this process by femtosecond XANES spectroscopy[15] and UV transient absorption experiments[16] confirm that the deactivation takes places through intermediate ^{3}MLCT states instead of ligand-field states, following a two-step intersystem-crossing process $^1MLCT \rightarrow {}^3MLCT \rightarrow {}^5T_2$. In these studies the different electronic states involved in the decay process could be identified by making use of the correlation of different spin states with the Fe–N distances, as shown in a previous theoretical study.[17]

Hence, theoretical studies emerge as a valuable tool to investigate the electronic states implied in the LIESST process and to validate proposed interconversion mechanisms based on experimental data. To achieve this goal, an accurate study of the potential energy surfaces of the different electronic states that could be involved in the LIESST mechanism is essential. Very recently, wave-function-based electronic structure calculations for various SCO systems[17,18] have been proven to describe the ground and excited spin states properly, as well as the spin-orbit coupling at the crossings between these states. The computational approach employed in these studies is based on multiconfigurational second-order perturbation theory (CASPT2)[19] and is able to characterize both ground state properties (molecular geometries, ΔE^0_{HL}, or vibrational frequencies) and properties related to the excited states such as the absorption/emission spectra, the nature of the excited states, or the location of intersystem crossings. Up to now, other methods based on density functional theory (DFT) have been successfully applied mainly to the study of structural parameters, vibrational frequencies and entropy variations between the HS and LS states.[20–22]

The aim of this work is to reach an accurate description at the molecular level of the different electronic states involved in the LS to HS transition mediated by light irradiation for the $[Fe^{II}(bpy)_3]^{2+}$ complex. CASPT2 calculations of the potential energy surfaces of all low-lying electronic states allow a quantitative representation of the Jablonski diagram for this system to be obtained. This representation plots the relative energy of the different electronic states as a function of the Fe–N distance. Based on this diagram, the optical spectra of the $[Fe^{II}(bpy)_3]^{2+}$ complex can be assessed, the energetic ordering of the various d–d ligand-field and MLCT states can be established, and the optimal Fe–N distance for each electronic state can be determined. This information is essential to elucidate the states involved in the LIESST mechanism and, therefore, it will help to unravel the role of the ligand-field and the MLCT states in the LS to HS conversion by light irradiation for the $[Fe^{II}(bpy)_3]^{2+}$ complex and related compounds in which the LIESST process is triggered by an MLCT excitation.

Experimental Section

Calculations were performed by applying the CASSCF/CASPT2[19] method (i.e., second-order perturbation theory based on a complete active space self-consistent field reference wave function), implemented in the MOLCAS 7.2 code.[23] The Cholesky decomposition was used to treat the two-electron integrals.[24,25] Scalar relativistic effects were included by using a Douglas–Kroll–Hess Hamiltonian.[26,27] Spin-orbit coupling was accounted for by the spin-orbit state interaction approach.[28,29] Within this approach, the CASSCF spin-free wave functions are used as a basis to construct the spin-orbit Hamiltonian. By diagonalizing this matrix, the energy of the different spin-orbit eigenstates can be obtained.

Three different active spaces have been used to obtain the CASSCF wave functions. The first active space contains ten electrons distributed among 12 orbitals, the five 3d Fe orbitals, a second formally empty d shell and two e-like σ-bonding ligand orbitals. This active space ensures a balanced description of two important effects: the dynamical electron correlation associated with the Fe 3d electrons[30,31] and the ligand-to-metal charge-transfer (LMCT) effects related to covalent metal–ligand interactions.[17,32] Hence, this active space allows both the metal-centered d–d states and the LMCT states to be properly described. To study the MLCT states, the active space has to include virtual ligand orbitals. Therefore, the previous active space has been extended with three ligand π^* orbitals, giving rise to an active space of ten electrons in 15 orbitals. Finally, to analyze the ligand-centered states, which are responsible for the intense absorption bands in the optical spectra of $[Fe^{II}(bpy)_3]^{2+}$ in solution, an active space containing 12 ligand orbitals (six occupied ligand π orbitals and six ligand π^* orbitals) and 12 electrons has been considered.

The CASSCF multiconfigurational wave functions account for nondynamical electron correlation. Subsequent CASPT2 calculations allow for the remaining, mainly atomic, electron correlation by correlating all the electrons except the deep core electrons (i.e., 1s for N and C and 1s2p for Fe).

The experimental geometry of the $[Fe^{II}(bpy)_3]^{2+}$ complex in the LS state is available from the crystallographic data of the $[Fe(bpy)_3](PF_6)_2$ compound at 293 K.[11] The complex presents a D_3 local symmetry as shown in Figure 1. Because a full geometry optimization of the system by using CASPT2 is computationally too demanding, the geometry of the complex in the LS and HS states has been optimized by DFT calculations using the B3LYP hybrid functional.[33–35] For the LS state, the value of the Fe–N distance obtained by B3LYP is 2.028 Å, in good agreement with previous theoretical studies of this system[22] and similar to the experimental

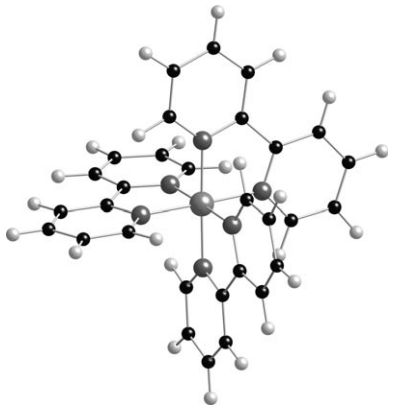

Figure 1. Ball-and-stick representation of the $[Fe^{II}(bpy)_3]^{2+}$ complex. The black spheres represent C, grey N, and light grey H. The central sphere represents Fe.

value of 1.967 Å. The optimized value of the N-Fe-N angle, 84.3°, is also close to the experimental value of 81.3°. The geometry optimization of the complex in the HS state leads to an enlargement of the Fe–N distances, whereas the internal coordinates of the rest of the complex remain almost unchanged; the B3LYP optimized value being 2.237 Å. The variation of the Fe–N distance under the spin transition is 0.21 Å.

Because the largest geometrical changes induced by the spin conversion occur for the Fe–N distance, usually the potential energy surfaces are plotted as a function of this single variable. However, for bidentate, and in general, multidentate ligands, the single variation of the Fe–N distance can result in strains in the structure of the complex. In such cases, it is more appropriate to define a coordinate that linearly interpolates between the geometry of the LS structure to the HS geometry as a variable to follow the spin conversion. Although this variable captures the variation of all the angles and distances of the complex, it predominantly describes the variation of the Fe–N distance. The representation of the CASPT2 potential energy curves along this coordinate allows the CASPT2 Fe–N equilibrium bond distance to be obtained. For the LS state, the optimized CASPT2 distance is 1.927 Å, similar to the value obtained by Pierloot et al.[32] and close to the experimental value, whereas for the HS the computed distance is 2.138 Å. As obtained from the geometry optimization by B3LYP calculations, an enlargement of 0.21 Å is observed under the spin conversion. This combined strategy, consisting of starting with a DFT-optimized structure and subsequently reoptimizing the crucial structure parameters at the CASPT2 level, has been successfully applied in other studies.[32,36,37]

All calculations have been performed within the abelian C_2 point group symmetry. For all atoms, atomic natural orbital basis sets, specifically designed to include relativistic effects, have been used.[38,39] The following contracted basis sets were applied: (7s, 6p, 5d, 4f, 3g, 2h) for Fe, (4s, 3p, 1d) for the N atoms bonded to the Fe, (3s, 2p) for the other N atoms and for C, and a (2s) contraction was used for H.

Results and Discussion

Equilibrium properties: First, the energy difference between the LS ($^1A_1$) and the HS ($^5T_2$) electronic states at the corresponding equilibrium geometry has been computed by CASPT2 calculations, based on an active space containing ten electrons and 12 orbitals. As mentioned in the previous section, the Fe–N distance obtained by CASPT2 increases from 1.927 Å for the LS to 2.138 Å for the HS state (i.e., around 0.2 Å as observed in other Fe^{II} materials). For this system, the LS is the ground state with a zero-point corrected energy difference, ΔE^0_{HL}, of 5807 cm^{-1}, in good agreement with the experimental estimate of approximately 6000 cm^{-1}. The character of the LS ground state can be assessed by analyzing the wave function in terms of valence-bond configurations based on atomic localized orbitals.[40] The LS state in its equilibrium geometry shows important covalent contributions due to the ligand σ-donation. About 41% of the wave function is due to single CT configurations (Fe $3d^7L^{-1}$) and 9% to double CT (Fe $3d^8L^{-2}$) contributions, and the influence of the non-CT configurations (Fe $3d^6$) is around 48%. The covalent character obtained for this system is larger than that found for Fe^{II} tetrazole-based complexes, for which the non-CT contributions showed a weight of 56%.[17] This difference in covalency can explain the larger value of the ΔE^0_{HL} for the $[Fe^{II}(bpy)_3]^{2+}$ complex compared with the SCO Fe^{II} tetrazole-based complexes in which the LS and HS states are very close in energy. In fact, it has been shown[41] that an increase in ligand σ-donation leads to a significant stabilization of the LS state and the associated enlargement of ΔE^0_{HL}. On the other hand, the HS state shows more ionic character and the wave function is dominated by non-CT configurations (82%), whereas the single CT configurations constitute approximately 15% of the wave function.

Absorption spectrum: The optical absorption spectrum of aqueous $[Fe^{II}(bpy)_3]^{2+}$ shows three main absorption bands.[42] The two low-lying bands are centered around 520 and 350 nm. These two broad bands have been assigned to MLCT transitions involving Fe (3d) orbitals and π^* ligand orbitals.[43,44] The UV part of the spectrum is dominated by ligand-centered transitions among the π and π^* orbitals of the bipyridine ligands. These excitations give rise to a very intense band between 200 and 300 nm. The metal-centered Fe d–d transitions are very weak because they are forbidden by the dipole selection rule and lie in the same energy region as the MLCT bands.

The absorption spectrum of the $[Fe^{II}(bpy)_3]^{2+}$ complex has been studied by computing the CASPT2 vertical transition energies from the LS equilibrium geometry and their corresponding relative intensities. Because the nature of the measured absorption bands are very different, different active spaces have been used to study the metal-centered Fe d–d, ligand-centered, and MLCT excitations, as explained in the previous section. By using an active space containing ten electrons in 15 orbitals, the lowest 16 singlet electronic states have been studied. These states include ^{1}MLCT, Fe d–d states, and states of mixed character. From all of them, the most intense excitations correspond to $^1A_1 \rightarrow {}^1$MLCT transitions involving an electron transfer from the Fe (3d) t_2 orbitals to the antibonding π^* ligand orbitals. There are several CT excitations of this kind that show different relative intensities. In Figure 2 each transition is represented by a Gaussian function centered at the corresponding computed vertical absorption energy in which the height denotes the relative intensity and the full-width at half maximum (FWHM) is

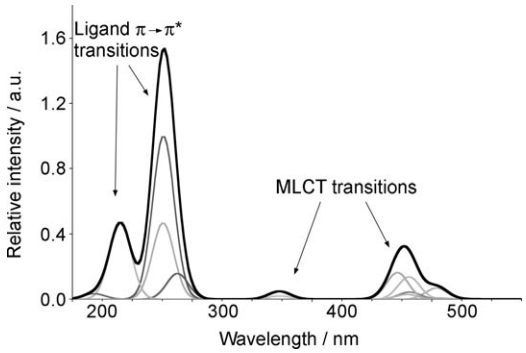

Figure 2. Theoretical absorption spectrum of $[Fe^{II}(bpy)_3]^{2+}$. Each transition is represented by a Gaussian function with a FWHM of 0.15 eV. The thick black line is the sum of the individual peaks. See the text for more details.

taken as 0.15 eV. This value has been chosen because it corresponds to the usual error bar of the CASPT2 method in computing transition energies. As can be seen in Figure 2, the excitations involving ^{1}MLCT states are arranged in two main bands, one centered around 460 nm and a second one, carrying less intensity, around 350 nm. The overall picture of the computed spectrum agrees with the experimental observation, although the maximum of the more intense band is shifted by approximately 50 nm to higher energies with respect to the experiment. The lowest Fe d–d transition corresponds to the $^1A_1 \rightarrow {}^1T_1$ excitation and occurs at 480 nm, hence it underlies the more intense ^{1}MLCT bands.

To study the ligand-centred excitations, the electronic distribution of the Fe^{II} atom in the LS state has been frozen and an active space exclusively containing ligand orbitals has been considered. In this way, the electronic transitions allowed uniquely involve π and π^* ligand orbitals and the size of the active space (12 orbitals and 12 electrons) keeps the calculations computationally feasible. CASPT2 calculations of the lowest low-lying singlet ligand-centered states show that these states indeed involve $\pi \rightarrow \pi^*$ excitations and clearly appear at higher energies compared with the ^{1}MLCT states. A very intense band with two components is found between 200–275 nm (see Figure 2), in agreement with the measured spectrum.[42] Because these excitations are localized in the π system of the pyridine rings, the values of the transition energies only depend on the local ligand geometry. In fact, we found a similar absorption spectrum of the gas-phase *cis* 2,2′-bipyridine molecule with the same geometry as in the complex.

Jablonski diagram: Up to this point, we have shown that the methodology applied in this study properly describes electronic states of different nature: metal-centered states, states involved in the ligand $\pi \rightarrow \pi^*$ transitions, and the more difficult MLCT states. The next step is to follow the evolution of the electronic states involved in the LIESST process as function of the geometrical changes induced by the irradiation that triggers the spin conversion. This procedure was successfully applied to study the potential energy curves in $[Fe(tz)_6]^{2+}$ (tz = tetrazole),[17] although no MLCT states were considered in that case. These states lie at significantly higher energy in the tetrazole compound than in the molecule studied here. The dependence of the relative energies of the different d^6 states is shown in Figure 3. The general shape of the curves is rather similar to those obtained in our previous study of the $[Fe(tz)_6]$ complex. The main difference lies in the relative position of the minima of HS and LS. They are nearly degenerate in the tetrazole complex, whereas there is a large difference of approximately 0.7 eV in $[Fe^{II}(bpy)_3]^{2+}$. The minimum of the excited singlet state ($^1T_1$) lies halfway between the minimum of the HS and LS states at d(Fe–N) = 2.01 Å. The curve of this excited singlet is nearly parallel to the curves of the two triplet states ($^3T_1$, $^3T_2$), and hence, no singlet–triplet crossing is observed.

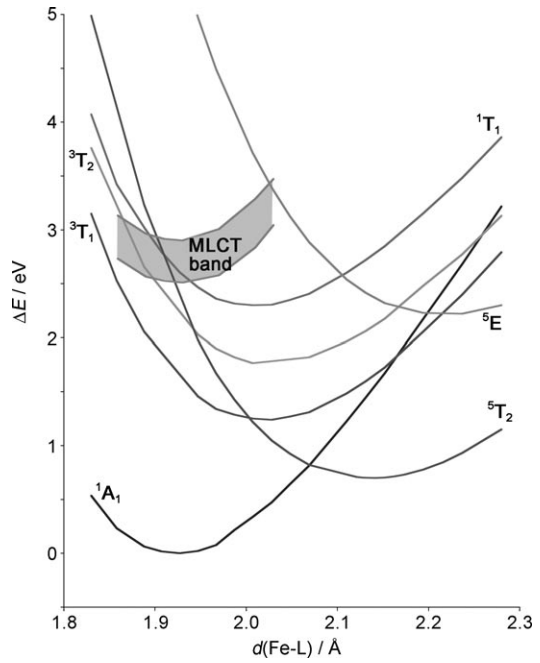

Figure 3. CASPT2 relative energies of the metal-centered d^6 states (thin lines) and the singlet and triplet MLCT states (grey band) as function of the Fe–ligand distance.

The participation of the MLCT states in the LIESST process requires a more involved strategy than for the simpler metal-centered d^6 states. As anticipated in the discussion of the absorption spectrum, the singlet MLCT manifold contains many states, it partially overlaps with the high-lying d^6 singlets, and has some states of mixed character, all in a small energy region. Therefore, it is not obvious how the different states can be followed when the complex evolves from the LS equilibrium geometry towards the HS geometry.

To solve this issue, we computed the absorption spectrum in the MLCT region at different geometries of the complex along the linear interpolation from the LS equilibrium geometry to the HS equilibrium geometry. The results are reflected in Figure 4, which shows the dispersion of the MLCT

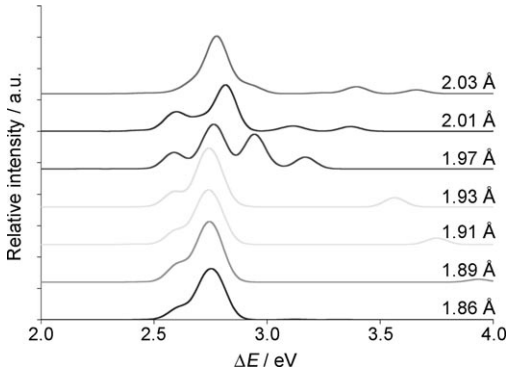

Figure 4. MLCT absorption band as function of the Fe–ligand distance. Each transition is represented by a Gaussian function with a FWHM of 0.15 eV. Absorption energies are relative to the $^1A_1$ state at each specific Fe–ligand distance.

bands with changing Fe–N distance. The energy of the $^1A_1$ state at each distance was used as a reference energy for each spectrum. Hence, we observe that the lowest, most intense MLCT band shows a rather similar energy dependence as the LS state, especially for distances around the LS equilibrium distance ($1.86 < R < 1.93$ Å). For larger distances the maximum of the band shifts to a slightly larger relative energy and there is a tendency for a certain widening of the band. A larger dispersion is found for the second, less intense MLCT band. It appears around 4.0 eV at $R = 1.89$ Å and is merged in the main peak around 1.97 Å.

Based on the dispersion found in Figure 4, the distance dependence of the singlet MLCT states is added to the Jablonski diagram as a broad band of approximately 0.4 eV instead of the lines used for the d^6 states. The minimum of this band appears at the same distance as for the LS state. Note that we consider both allowed and symmetry-forbidden MLCT states. There are no MLCT states below the uprise at approximately 2.5 eV in Figure 4. This means that the bottom of the MLCT band drawn in Figure 3 is the real lower limit for ^{1}MLCT states, both for the optically allowed and for the forbidden states, which can in principle both participate in the deactivation process.

We have also calculated the triplet-coupled MLCT states. As for the ^{1}MLCT, several states of similar character lie in a small energy range. The intensity of these states is very small because the direct excitation process from the LS ground state ($^1A_1$) involves a change of the spin, which is only weakly allowed through spin-orbit coupling. Hence, we cannot follow the evolution of the triplet MLCT states in the same way as for the singlet MLCT states. However, we observed that the ^{3}MLCT states appear in the same energy region as the ^{1}MLCT and the energies exactly follow the changes with the Fe–ligand distance observed for the ^{1}MLCT states. This is explained by the fact that the electronic configuration of the singlet- and triplet-coupled MLCT states is the same (formally Fe $3d^5L^{+1}$), and hence, the energy difference between these states is largely determined by the intersite exchange integral K of the unpaired electron in the π^* ligand orbital and an electron in an Fe 3d orbital. This intersite exchange integral only contributes to the triplet MLCT state, but is much smaller than the intrasite K, responsible for the $^1T_1$–$^3T_2$ energy difference.[18] Based on these findings, we assume that the MLCT band in Figure 3 represents both the singlet and the triplet MLCT states. Similar equilibrium distances for singlet and triplet MLCT states are in line with the experimentally observed equilibrium distances for these states in the $[Ru(bpy)_3]^{2+}$ molecule.[45]

The current understanding of the deactivation of the ^{1}MLCT state to the metastable HS state involves a fast singlet to triplet transformation in the MLCT manifold, followed by the decay into highly excited vibrational levels of the HS state, to end up in the HS minimum by radiationless decay. Our Jablonski diagram confirms the possibility of such a mechanism. The singlet and triplet MLCT states largely overlap in energy and the spin-orbit coupling between these states is significant. We calculated a spin-orbit interaction of the order of 200 cm^{-1} for the different MLCT states. The subsequent intersystem crossing to the HS state can take place in the same geometry region, because the $^5T_2$ state crosses the MLCT band near the minimum of the initial LS state. The spin-orbit interaction between ^{3}MLCT and $^5T_2$ is smaller than the ^{1,3}MLCT spin orbit interactions. However, the near-degeneracy of the ^{3}MLCT and $^5T_2$ states in the Franck–Condon region makes this conversion possible. Once the HS is populated, the system decays relatively fast to the LS, in line with the computed energy barrier for the HS→LS relaxation of only 800 cm^{-1}.

Conclusion

The structural and electronic properties related to the SCO process in $[Fe^{II}(bpy)_3]^{2+}$ have been studied with CASPT2. The mechanism of LIESST in this complex has recently been addressed in several experimental papers and it was proposed that the deactivation of the excited singlet state occurs through an intermediate ^{3}MLCT state before the final (metastable) HS state is populated. Our computational study provides additional evidence for this hypothesis by analyzing the energy dependence of the relevant electronic states on the changes in the geometry caused by the LS–HS conversion. Relevant parameters such as the difference in the Fe–N distance in the HS and LS state, the HS–LS energy difference, and the absorption spectrum are in agreement with the available experimental data.

Our calculations indicate that the MLCT band is a superposition of many states, mainly of MLCT character but states of Fe $3d^6$ or mixed d^6/MLCT character are also found in this region. By following the dispersion of the most intense singlet MLCT band with changing Fe–N distance, we could construct a curve that represents the potential energy surface of the collection of ^{1}MLCT states and add it to the standard Jablonski diagram. The curve is represented by a broad band of approximately 0.4 eV to reflect the energy range in which ^{1}MLCT states can be found. The ^{3}MLCT states are found in the same energy interval and the singlet–triplet conversion is further favored by a rather strong spin-orbit coupling element between the ^{1}MLCT and ^{3}MLCT states. Finally, we found that the HS state crosses the MLCT band in the Jablonski diagram exactly in the Franck–Condon region. This could lead to an extremely fast deactivation of the ^{1}MLCT state into the HS state, intermediated by the ^{3}MLCT state.

The question of the high efficiency of the spin conversion process remains. The crossing of the $^5T_2$ state and the MLCT states in the Franck–Condon region shown in Figure 3 explains why the triplet–quintet conversion can take place at very small time scales. However, the same figure shows that some ligand-field states (e.g., $^3T_2$ and $^1T_1$) cross in the same region. An inspection of the spin-orbit coupling matrix reveals that the coupling between ^{3}MLCT states and the ligand-field states is small, $< 75\ cm^{-1}$. This would point to the possibility that the excited ^{3}MLCT state could also decay into other states than the $^5T_2$. Unfortunately, we do not have a definite answer to this question yet, but in favor of the decay through the $^5T_2$ state is the more ionic character of this state in comparison with the triplet and singlet ligand states. The formal electronic configuration of the MLCT states is Fe $3d^5L^{+1}$, whereas the more ionic ligand-field states are Fe $3d^6L$. On the other hand, the triplet and singlet ligand-field states have important contributions from the Fe $3d^7L^{-1}$ electronic configurations. This could lead to a more effective decay of the ^{3}MLCT into the more similar $^5T_2$ state (single electron transfer) than through the triplet or singlet ligand states, which require a certain degree of double electron transfer.

Acknowledgements

Financial support has been provided by the Spanish Ministry for Science and Innovation (Project FIS2008-02238 and CTQ2008-06644-C02-01), and the Generalitat de Catalunya (2009SGR-1041, 2009SGR-462, XRQTC)

[1] *Spin crossover in Transition Metal Compounds, Vols. 233–235* (Eds.: P. Gütlich, H. A. Goodwin), Springer, Berlin, **2004**.
[2] P. Gütlich, H. A. Goodwin in *Spin crossover in Transition Metal Compounds I, Vol. 233* (Eds.: P. Gütlich, H. A. Goodwin), Springer, Berlin, **2004**, pp. 1–47.
[3] A. Hauser in *Spin crossover in Transition Metal Compounds I, Vol. 233* (Eds.: P. Gütlich, H. A. Goodwin), Springer: Berlin, **2004**, pp. 49–58.
[4] S. Decurtins, P. Gütlich, C. P. Kohler, H. Spiering, A. Hauser, *Chem. Phys. Lett.* **1984**, *105*, 1–4.
[5] S. Decurtins, P. Gütlich, C. P. Kohler, H. Spiering, *J. Chem. Soc. Chem. Commun.* **1985**, 430–432.
[6] A. Hauser, *J. Chem. Phys.* **1991**, *94*, 2741–2748.
[7] A. Hauser in *Spin crossover in Transition Metal Compounds II, Vol. 234* (Eds.: P. Gütlich, H. A. Goodwin), Springer, Berlin, **2004**, pp. 155–198.
[8] P. Guionneau, M. Marchivie, G. Bravic, J. F. Letard, D. Chasseau in *Spin crossover in Transition Metal Compounds II, Vol. 234* (Eds.: P. Gütlich, H. A. Goodwin), Springer, Berlin, **2004**, pp. 97–128.
[9] C. Brady, J. J. McGarvey, J. K. McCusker, H. Toftlund, D. N. Hendrickson in *Spin crossover in Transition Metal Compounds III, Vol. 235* (Eds.: P. Gütlich, H. A. Goodwin), Springer-, Berlin, **2004**, pp. 1–22.
[10] J. K. McCusker, K. N. Walda, R. C. Dunn, J. D. Simon, D. Magde, D. N. Hendrickson, *J. Am. Chem. Soc.* **1992**, *114*, 6919–6920.
[11] S. Dick, *Z. Kristallogr. New Cryst. Struct.* **1998**, 213, 356.
[12] W. Gawelda, V.-T. Pham, M. Benfatto, Y. Zaushit *syn*, M. Kaiser, D. Grolimund, S. L. Johnson, R. Abela, A. Hauser, C. Bressler, M. Chergui, *Phys. Rev. Lett.* **2007**, 98, 057401.
[13] W. Gawelda, V.-T. Pham, R. M. van der Veen, D. Grolimund, R. Abela, M. Chergui, C. Bressler, *J. Chem. Phys.* **2009**, *130*, 124520.
[14] W. Gawelda, A. Cannizzo, V.-T. Pham, F. van Mourik, C. Bressler, M. Chergui, *J. Am. Chem. Soc.* **2007**, *129*, 8199–8206.
[15] C. Bressler, C. Milne, V.-T. Pham, A. ElNahhas, R. M. van der Veen, W. Gawelda, S. L. Johnson, P. Beaud, D. Grolimund, M. Kaiser, C. N. Borca, G. Ingold, R. Abela, M. Chergui, *Science* **2009**, *323*, 489–492.
[16] C. Consani, M. Prémont-Schwarz, A. ElNahhas, C. Bressler, F. van Mourik, A. Cannizzo, M. Chergui, *Angew. Chem.* **2009**, *121*, 7320; *Angew. Chem. Int. Ed.* **2009**, *48*, 7184–7187.
[17] B. Ordejón, C. de Graaf, C. Sousa, *J. Am. Chem. Soc.* **2008**, *130*, 13961–13968.
[18] N. Suaud, M.-L. Bonnet, C. Boilleau, P. Labèguerie, N. Guihéry, *J. Am. Chem. Soc.* **2009**, *131*, 715–722.
[19] K. Andersson, P.-Å. Malmqvist, B. O. Roos, *J. Chem. Phys.* **1992**, *96*, 1218–1226.
[20] H. Paulsen, A. X. Trautwein in *Spin crossover in Transition Metal Compounds III, Vol. 235* (Eds.: P. Gütlich H. A. Goodwin), Springer, Berlin, **2004**, pp. 197–219.
[21] J. A. Wolny, H. Paulsen, A. X. Trautwein, V. Schünemann, *Coord. Chem. Rev.* **2009**, *253*, 2423–2431.
[22] L. M. Lawson Daku, A. Vargas, A. Hauser, A. Fouqueau, M. E. Casida, *ChemPhysChem* **2005**, *6*, 1393–1410.
[23] G. Karlström, R. Lindh, P.-Å. Malmqvist, B. O. Roos, U. Ryde, V. Veryazov, P.-O. Widmark, M. Cossi, B. Schimmelpfennig, P. Neogrady, L. Seijo, *Comput. Mater. Sci.* **2003**, *28*, 222–239.
[24] F. Aquilante, T. B. Pedersen, R. Lindh, *J. Chem. Phys.* **2007**, *126*, 194106.
[25] F. Aquilante, P.-Å. Malmqvist, T. B. Pedersen, A. Ghosh, B. O. Roos, *J. Chem. Theory Comput.* **2008**, *4*, 694–702.
[26] N. Douglas, N. M. Kroll, *Ann. Phys.* **1974**, *82*, 89–155.
[27] B. Hess, *Phys. Rev. A* **1986**, *33*, 3742.
[28] P.-Å. Malmqvist, B. O. Roos, B. Schimmelpfennig, *Chem. Phys. Lett.* **2002**, *357*, 230–240.
[29] B. O. Roos, P.-Å. Malmqvist, *Phys. Chem. Chem. Phys.* **2004**, *6*, 2919–2927.
[30] K. Andersson, B. O. Roos, *Chem. Phys. Lett.* **1992**, *191*, 507–514.
[31] C. de Graaf, R. Broer, W. C. Nieuwpoort, *Chem. Phys.* **1996**, *208*, 35–43.
[32] K. Pierloot, S. Vancoillie, *J. Chem. Phys.* **2006**, *125*, 124303.
[33] C. Lee, W. Yang, R. G. Parr, *Phys. Rev. B* **1988**, *37*, 785–789.
[34] A. D. Becke, *J. Chem. Phys.* **1993**, *98*, 5648–5652.
[35] S. H. Vosko, L. Wilk, M. Nusair, *Can. J. Phys.* **1980**, *58*, 1200–1211.
[36] K. Pierloot, A. Delabie, M. H. Groothaert, R. A. Schoonheydt, *Phys. Chem. Chem. Phys.* **2001**, *3*, 2174–2183.
[37] K. R. F. Somers, A. Ceulemans, *J. Phys. Chem. A* **2004**, *108*, 7577–7583.

[38] B. O. Roos, R. Lindh, P.-Å. Malmqvist, V. Veryazov, P.-O. Widmark, *J. Phys. Chem. A* **2005**, *109*, 6575–6579.
[39] B. O. Roos, R. Lindh, P.-Å. Malmqvist, V. Veryazov, P.-O. Widmark, *J. Phys. Chem. A* **2004**, *108*, 2851–2858.
[40] A. Sadoc, C. de Graaf, R. Broer, *Phys. Rev. B* **2007**, *75*, 165116.
[41] A. Domingo, M. A. Carvajal, C. de Graaf, *Int. J. Quantum Chem.* **2010**, *110*, 331–337.
[42] S. Decurtins, F. Felix, J. Ferguson, H. U. Güdel, A. Ludi, *J. Am. Chem. Soc.* **1980**, *102*, 4102–4106.
[43] E. M. Kober, T. J. Meyer, *Inorg. Chem.* **1982**, *21*, 3967–3977.
[44] R. M. Berger, D. R. McMillin, *Inorg. Chim. Acta* **1990**, *177*, 65–69.
[45] W. Gawelda, M. Johnson, F. M. F. de Groot, R. Abela, C. Bressler, M. Chergui, *J. Am. Chem. Soc.* **2006**, *128*, 5001–5009.

Received: December 14, 2009
Published online: March 12, 2010

